Energy Performances of Tensile Material in Building Renovation in the Nordic Region

Giovanni Ciampi[1], Yorgos Spanodimitriou[1], Alessandro Nocente[2*], Michelangelo Scorpio[1], Sergio Sibilio[1]

[1]Università della Campania "L. Vanvitelli", Aversa (CE), Italy
[2]SINTEF AS, Trondheim, Norway
***** *corresponding author: alessandro.nocente@sintef.no*

Abstract

Tensile materials are increasingly used in the building envelope as second-skin systems, despite a lack of investigation on their effects. In this work, a second-skin system integrating a tensile material as an outer layer has been adopted in the retrofit analysis of two of the most common building typologies in the Norwegian context. The simulations were carried out by implementing a custom control logic for the system, considering the outdoor air temperature and the global vertical irradiation on the façades. The proposed retrofit solution allowed for a primary energy saving of about 35%.

Introduction

Buildings currently account for about 40% of the global energy use, constituting approximately 36% of the overall global carbon emissions (European Commission, 2018). The European Union (EU) has set targets to progressively reduce greenhouse gas emissions by 2050 (European Commission, 2021). The vast majority of the existing non-residential EU building stock has been built before 1990, and almost 55% of this stock has yet to be renovated (Boermans et al., 2012; Schimschar et al., 2011); in particular, according to (Nord et al., 2021), about 96.8% of Norwegian building stock was classified as old building (before 1980) or medium-aged building (1981–2010). Therefore, building retrofit actions are more and more fostered by the government to encourage the improvement of the overall building energy efficiency. These energy efficiency retrofit actions can be classified into active or passive (Chen et al., 2020; Ciampi et al., 2021b; Diallo et al., 2017). Active actions include installing different active technologies, while passive actions aim either to manage better the thermal gains and energy losses of the building or to increase the use of natural lighting, heating, and cooling. Intuitively, the building envelope plays a crucial role in the effectiveness of passive actions (Chen et al., 2020). However, it is not always possible to replace the glazing or upgrade the insulation layers of the envelope, considering the complexity due to, for example, the historical relevance of a building or the cost efficiency for the stakeholders (Ciampi et al., 2021b). In these cases, a lightweight, non-impacting, and low-maintenance solution, such as installing an external second-skin (SS) layer on the façade, can be considered as a foreseeable passive solution to improve the thermal performance of the building envelope. In addition, the SS systems seem to offer a good compromise in terms of ease of installation, performance, and cost-effectiveness (Ciampi et al., 2021b). The SS system consists of an additional second-skin layer hung on the surface of the external building wall, with an air cavity in-between. Consequently, the SS systems are well suited to adopt new materials as an SS layer, this thanks to their simple structure. In the last decade, several studies have been carried out to evaluate the potential benefit achievable by using SS systems realized with opaque (also phase change panels) and transparent materials used as SS external layer (de Gracia et al., 2015; Gelesz et al., 2020; Gruner & Haase, 2012; Naboni & Tarantino, 2014; Poirazis, 2004; Saad & Araji, 2020; Shahrzad & Umberto, 2022; Soudian & Berardi, 2021). In general, the literature review highlights a gap in the investigation of the SS system in cold climates, with a total lack of studies on tensile materials at high latitudes. However, the integration of tensile in the contemporary architecture panorama is more and more common (CORDIS - European Commission; Facid North America; Serge Ferrari, a-b) thanks to the lightness, flexibility, and customizability of such material. Indeed, tensile and membrane-like materials are well-suited for both new and existing buildings, providing thermal comfort through passive cooling/heating and thus reducing the energy consumption and the greenhouse gas emissions (Chiu & Lin, 2015; Lehrer, 2011; Poirazis, 2004).

The aim of this paper is to evaluate the energy impact of passive retrofit actions on a typical office building in terms of primary energy saving, proposing a general operational methodology and highlighting best practices for the Nordic climate to cover the gaps in this Region. The analysis was carried out by means of the dynamic simulation software TRNSYS across a whole year using experimental weather data, comparing the results of a reference office building with those achievable by adopting a passive retrofit action on the building envelope. In particular, the refurbishment consists of the installation of a SS system integrating a tensile material (Serge Ferrari, a) as a light SS layer, without the need for invasive interventions on the façade of the reference building. Different arrangements of the SS system have been considered upon varying the (i) building orientation, (ii) the building age, and (iii) the control logic for both the

air cavity shutters as well as the SS façade sections on the windows. The energy performance of the SS system has been assessed in the Nordic climate using experimental weather data acquired over a whole year. The simulation results allowed to evaluate the primary energy saving compared to the current status of the buildings assumed as benchmarks.

Numerical model

The study is focused on an office building. It aims to propose a general operational methodology and highlight a best practice for retrofit actions in the Norwegian context. The software TRNSYS 18 was used to evaluate the potential benefit achievable in an office building refurbishment using a tensile material (a PVC-coated polyester fabric) as the outer layer in a SS system in terms of primary energy saving and reduction of carbon dioxide equivalent emissions. The reference building investigated in this research has been modeled in SketchUp 3D-modeling software based on a "typical" office building from the IEA Annex 27 activity (Köhl, 2007). It is a seven-story building 45.9 m wide, 14.4 m deep, and 28.9 m tall. The building has been simulated considering two different orientations for the two main façades, north-south (Figure 1a) and east-west (Figure1b).

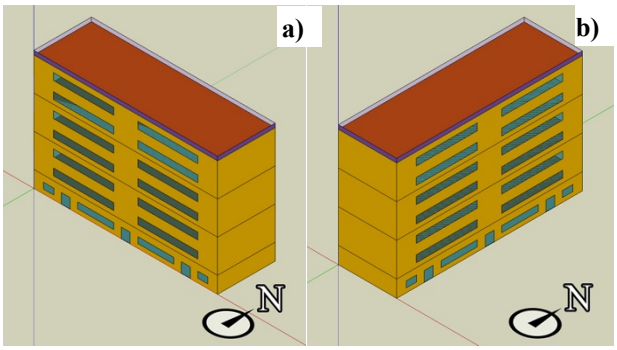

Figure 1. Axonometric view of the building model in two orientations: a) north-south and b) east-west.

The windows were implemented only on the two main façades considering the optimal Windows-to-Wall Ratio (WWR) as suggested by (Goia, 2016) and reported in Table 1. The geometrical model has been then imported into TRNSYS in order to characterize the envelope (all surfaces are modeled as massless), the internal gains, and the setpoint for the cooling and heating systems. The study was carried out considered the building located in Trondheim (63° 26′ 24″ N, 10° 24′ 0″ E), central Norway.

Table 1: Optimal WWR for the two main façades upon varying the building orientation (Goia, 2016).

North-south orientation		**East-west orientation**	
North façade	South façade	East façade	West façade
0.37	0.27	0.33	0.34

The two most common building typologies of Norwegian building stock have been modeled as reference buildings (Nord et al., 2021), classified as old building (built before 1980) or medium-aged building (built between 1981 and 2010). The envelope of these two building typologies has been characterized differently in terms of thermal transmittance (U-value), according to their age and contemporary building regulation (Nord et al., 2021). Table 2 summarizes the implemented U-values.

Table 2. Summary of the considered U-values.

Reference case	**Construction period**	**Construction**	**U-values (W/m^2K)**
RC1 (based on Enova, 2004)	Before 1980	External Wall	0.50
		Roof	0.40
		Floor	0.40
		Windows	2.89
		Doors	2.00
RC2 (based on TEK87/97, Direktoratet for byggkvalitet)	1981-2010	Wall	0.30
		Roof	0.20
		Floor	0.30
		Windows	2.40
		Doors	2.00

In TRNSYS, the reference building has been simulated through Type 56. Table 3 reports the common simulation parameters (EN12831, 2003; G.I. Industrial Holding, 2022; Goia, 2016; UNI/TS 11300-1, 2014). In addition, experimental data acquired from June 1st (2021) to May 31st (2022) were used to take into account the real weather condition. Data were acquired by the weather station integrated into the ZEB Test Cell experimental facility in Trondheim. The experimental weather conditions were acquired with one-minute temporal resolution and averaged over 15 minutes. Figure 2 reports the maximum (T_{MAX}), minimum (T_{MIN}), and average (T_{AVG}) values of the outdoor air temperature as well as the average global horizontal irradiation (G_{AVG}) upon varying the month. This figure highlights that: (i) the outdoor air temperature ranges between a minimum of -18.75 °C in February and a maximum of 30.94 °C in June, (ii) the average global horizontal irradiation is minimum in December (9.72 W/m^2), while the value of G_{AVG} is maximum in June (275.31 W/m^2). In addition, the experimental weather data shows that July 2021 was particularly cloudy.

Table 3. Summary of the simulations' parameters.

Parameter	**Detail**	**Value**
Occupancy	Workhours	8:00-11:30 12:30-16:00
Heating system	Temperature setpoint	19 °C
	COP	2.81
Cooling system	Temperature setpoint	26 °C
	EER	2.39
Lighting system	Workhours	8.0 W/m^2
	Lunchbreak	2.4 W/m^2
	Nighttime/weekend	0.0 W/m^2
Equipment	Workhours	11.0 W/m^2
	Lunchbreak	6.6 W/m^2
	Nighttime/weekend	1.1 W/m^2
People	Workhours	7.0 W/m^2
	Lunchbreak	2.1 W/m^2
	Nighttime/weekend	0.0 W/m^2

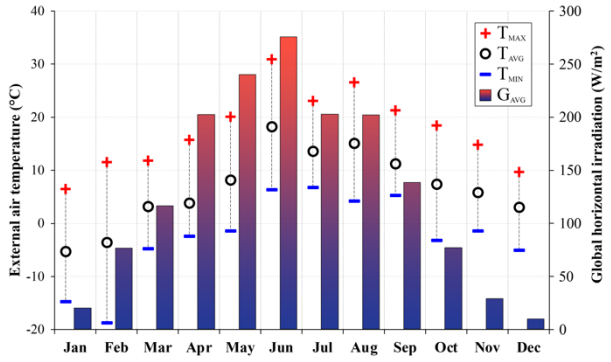

Figure 2. Values of T_{MAX}, T_{MIN}, T_{AVG}, and G_{AVG} for each simulation month.

A preliminary simulation set was run in order to assess the thermal and cooling loads across the whole year for both buildings' typologies and orientations to choose a proper size for the heating and cooling systems. Thus, four commercial parallel-connected electric heat pump (G.I. Industrial Holding) devices, coupled with a multi-split air conditioning system, have been implemented for each flat to supply the required heating and cooling energy. In the refurbishment cases, a SS system (consisting of the SS external layer, a 10cm wide air cavity, and an insulation layer on the outer surface of the existing exterior wall) integrating the tensile material as the external layer has been implemented on the whole reference building's walls, in both orientations. The other surfaces were left as in the original reference cases. The SS system was implemented in TRNSYS through the Type 1230. This TRNSYS Type coupled with Type 56 reproduces the behavior of the external second-skin layer with the 10 cm wide air cavity. In particular, the external layer of the building wall (modeled with Type 56), usually an insulation layer, acts as an interface layer between the two Types by coupling its temperature and thermal resistance to model the wall heat transfer. Type 1230 considers: (i) the solar radiation, the long wave radiation, and the air convection on the external surface of the outside layer; (ii) the energy storage and the conduction in the outside layer; (iii) radiation exchange between the outside layer and the air cavity; (iv) the convective exchanges from all the surfaces facing in the air cavity; (v) the conduction through the interface layer. Additional details about the Type 1230 are reported in (Ciampi et al., 2021a, 2021b). In particular, in (Ciampi et al., 2021b), the authors validated the simulation model of the SS system used in this work based on experimental data acquired in the south Italian climate. The comparison between the experimental and the numerical data showed good reliability of this numerical model, with an RMSE of 0.5 °C and 0.4 °C for the indoor air temperature and the temperature of the air cavity, respectively (Ciampi et al., 2021b). In this paper, the insulation layer (Expanded PolyStyrene - EPS, λ = 0.041 W/mK) has been set differently upon varying building ages in order to reach the U-value thresholds highlighted by the current legislation on the performance of the building envelope (TEK 17, Direktoratet for byggkvalitet). Table 4 reports a summary of the simulation cases, highlighting the different insulation layer thicknesses (s_{EPS}), the U-values of external vertical walls in the Reference Cases (RCs) and Proposed Cases (PCs), and the different global vertical radiation (G_{vi}) thresholds implemented in the SS system control strategies for the PCs. Six different G_{vi} threshold values have been considered (50, 100, 150, 200, 250, and 300 W/m^2).

Table 4: Summary of the case studies.

Case study	**Main façades orientation**	**s_{EPS} (m)**	**Walls U-value (W/m^{2}K)**	**G_{vi} (W/m^2)**
RC1a	North-south	-	0.50	-
RC1b	East-west			
PC1a_50	North-south	0.098	0.22	50
PC1a_100				100
PC1a_150				150
PC1a_200				200
PC1a_250				250
PC1a_300				300
PC1b_50	East-west	0.098	0.22	50
PC1b_100				100
PC1b_150				150
PC1b_200				200
PC1b_250				250
PC1b_300				300
RC2a	North-south	-	0.30	-
RC2b	East-west			
PC2a_50	North-south	0.043	0.22	50
PC2a_100				100
PC2a_150				150
PC2a_200				200
PC2a_250				250
PC2a_300				300
PC2b_50	East-west	0.043	0.22	50
PC2b_100				100
PC2b_150				150
PC2b_200				200
PC2b_250				250
PC2b_300				300

To take advantage of the characteristics of the polyester fabric, which allows for the see-through, the SS external layer has been placed on the whole façade (Figure 3), including the windows. The SS sections in front of the windows are operated independently on each façade to regulate the solar gains (Figure 3): they are kept open when the G_{vi} values are lower than the threshold and closed when G_{vi} values are higher. Shutters regulate the airflow in the SS air cavity at the inlet and the outlet, keeping the cavity closed when the outdoor air temperature is higher than 20 °C and opening them when the temperature exceeds this value to maximize ventilation. Considering these two control logics, four different operating states have been assumed, which affect the air infiltration rates from the outdoor to the indoor through the building envelope.

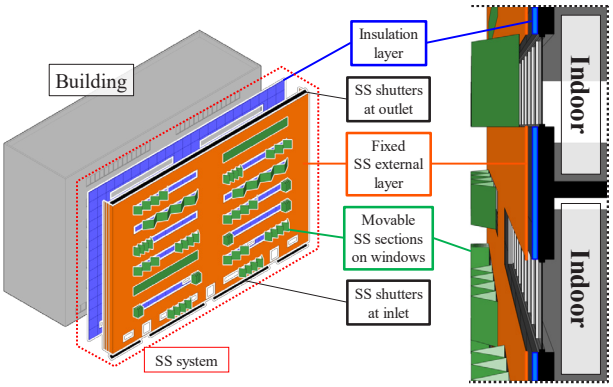

Figure 3. Axonometry (left) and section (right) of the building with the proposed SS system.

In this study, the changes in infiltration rates were assumed on the basis of literature references (Cho & Kim, 2013; Dickson, 2004): (i) both the SS sections in front of the windows and the shutters are open, so the air infiltration rate in the PCs is equal to the RCs one (4 m^3/h, Nord et al., 2021); (ii) both are closed, so the air infiltration rate in the PCs is lower than the RCs one (0.6 m^3/h); (iii) one is open while the other is closed, so the infiltration rate in the PCs is a lower than the RCs one but higher than the previous case (2.3 m^3/h). These assumptions could be the main limitation of this work. As stated in (Darvish et al., 2020), the air infiltration through the envelope, due to the difference between the pressure inside the building and the pressure on its façade, can be significantly influenced by modifying the envelope shape and composition. In this regard, the study presented in this work serves as the first step of a possible broader experimental study: at the moment, only the experimental weather data was available for such a northern location, while the numerical model for the SS system integrating the tensile material was developed and validated in the south European area (Ciampi et al., 2021b). Further experimental analysis is required in the Nordic Region to assess the influence of different boundary conditions and the effects on the overall balance from a fluid-dynamic point of view too. A summary of the operating status and the combination of the implemented logic is reported in Table 5.

Table 5: Summary of the SS system operating states.

Operating status	**SS sections on windows**	**SS shutters of the cavity**	**Infiltration rate through the building envelope (m^3/h)**
Op. 1	Open ($G_v < G_{vi}$)	Open ($T_{air} > 20$ °C)	4.0
Op. 2	Closed ($G_v \geq G_{vi}$)	Closed ($T_{air} \leq 20$ °C)	0.6
Op. 3	Open ($G_v < G_{vi}$)	Closed ($T_{air} \leq 20$ °C)	2.3
Op. 4	Closed ($G_v \geq G_{vi}$)	Open ($T_{air} > 20$ °C)	2.3

Methods of analysis

The energy comparison between the PCs and the RCs has been performed considering the primary energy consumption through the index PES (Primary Energy Saving) (Ciampi et al., 2021b; Roselli et al., 2020):

$$PES = \left[\left(E_p^{RC} - E_p^{PC}\right) \Big/ E_p^{RC}\right] \quad (1)$$

where E_p^{RC} is the primary energy associated with the reference cases (RC1a, RC1b, RC2a, and RC2b, see Table 4), while E_p^{PC} is the primary energy associated with each proposed case (PC1a, PC1b, PC2a, and PC2b, Table 4). A positive PES index value indicates that the proposed refurbishment actions allow for a primary energy reduction compared to the reference case.

The values of the E_p^{RC} and E_p^{PC} are calculated as reported below:

$$E_p^{RC} = \left(\frac{E_{th}^{RC}}{COP} + \frac{E_{cool}^{RC}}{EER} + E_{el,equipment} + E_{el,lighting}\right) \Big/ \eta_{PP} \quad (2)$$

$$E_p^{PC} = \left(\frac{E_{th}^{PC}}{COP} + \frac{E_{cool}^{PC}}{EER} + E_{el,equipment} + E_{el,lighting}\right) \Big/ \eta_{PP} \quad (3)$$

where η_{PP} is the power plants' average efficiency. The value of η_{PP} is assumed equal to 0.78 according to (European Environment Agency, 2021), while the values of COP and EER are reported in Table 3.

Simulation Results

Before carrying out an energy impact assessment of passive retrofit actions proposed in Table 4, a preliminary analysis was carried out considering a simulation set on the same RC1 and RC2 buildings while adopting only a traditional retrofit action involving the installation of an insulation layer on the outer surface of the external wall. The insulation layer's thickness was set to satisfy the external walls' thermal transmittance values requested by the Norwegian building regulation code (TEK 17, Direktoratet for byggkvalitet). These four preliminary simulations (two for each case, in both orientations) returned minimal gains in terms of PES, equal to 2.05% and 0.62% for the first (before 1980) and the second (1981-2010) reference building, respectively. Then, the 28 simulation case studies were carried out. Figure 4 and Table 6 report the 28 simulation case studies. In particular, Figure 4 shows the values of PES (cfr. Eq. 1) upon varying the case study, while Table 6 reports the heating and cooling energy flows associated with the whole building upon varying the case study and the month. In Figure 4, the black bars report the results for the retrofit on the first reference building (built before 1980), while the red ones report the results for the second reference building (built between 1981 and 2010). Additionally, for both colors, the striped bars report the

results for the north-south oriented cases, while the solid filled bars report the east-west oriented ones. Finally, in Table 6, the values associated with the thermal energy flows are in red, while those associated with the cooling energy are in blue; the shade of the colors gets more intense as the values get higher in each case study and across all the case studies of the same typology (building type and orientation).

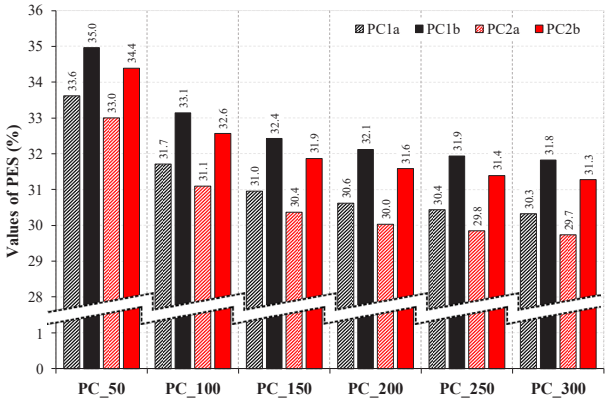

Figure 4. Values of PES varying the prosed case study.

The results reported in Figures 4 and in Table 6 highlight that:

- whatever the building orientation is, all the proposed cases (PC1 and PC2, Table 4) allow for a reduction of the primary energy consumption in comparison to the RC for each location (RC1 and RC2, Table 4), ranging between a minimum of 29.7% (PC2a_300) and a maximum of 35.0% (PC1b_50);
- whatever the control logic is, the proposed SS system returns better results in terms of primary energy saving when the building is east-west oriented (PC1b and PC2b, Table 4); in particular, in these cases, comparing the simulation results of the proposed case with those associated with the first reference building typology, the value of PES are always greater than 31.8% with a related reduction of thermal and cooling energy demand of about 36.7% and 31.3%, respectively (Table 6);
- whatever the reference building typology is, the adoption of the SS system always allows for a sensible improvement in terms of thermal energy demand with respect to the reference cases, achieving the best results when the G_{vi} threshold is set to 50 W/m^2;
- in the north-south oriented cases (RC1a and RC2a, Table 4), the cooling energy demand is reduced only when the G_{vi} threshold was equal to 200, 250 and 300 W/m^2, while in the east-west oriented ones (RC1b and RC2b, Table 4) the same is valid also for the 150 W/m^2 threshold value;
- the 250 W/m^2 control threshold (RC1a_250, RC1b_250, RC2a_250, and RC2b_250, Table 4) returns the best-balanced results in terms of both cooling and thermal energy reduction.

Figure 5 reports the monthly specific energy flows for building envelope in steady-state conditions associated with RC1b and PC1b_50 numerical case studies.

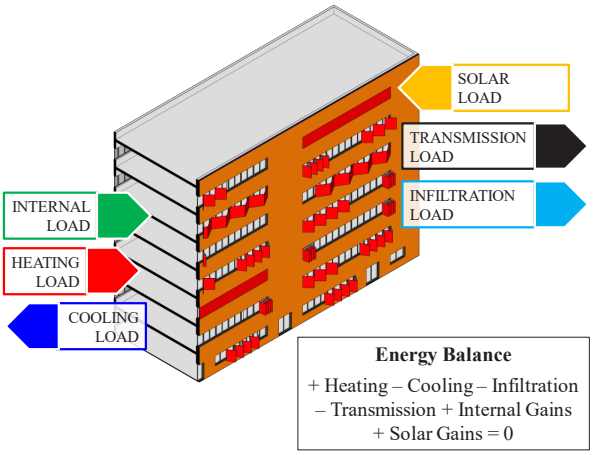

Month	Specific energy flows - RC1b - Reference case (kWh/m^2)					
	Heating load	Cooling load	Infiltration load	Transmission load	Internal load	Solar load
Jan	110.2	0.0	101.0	14.5	5.1	0.2
Feb	91.5	0.0	84.7	12.7	4.4	1.5
Mar	69.4	0.0	65.7	11.0	4.9	2.4
Apr	61.4	0.0	61.3	9.9	4.7	5.1
May	42.8	0.0	46.6	7.8	5.1	6.6
Jun	10.3	4.8	14.1	3.7	4.7	7.7
Jul	19.8	0.2	26.1	4.3	4.9	5.9
Aug	16.5	0.9	22.3	3.7	5.1	5.2
Sep	29.7	0.0	32.4	4.6	4.5	2.9
Oct	49.2	0.0	48.7	6.9	5.1	1.4
Nov	56.1	0.0	53.2	8.0	4.8	0.3
Dec	71.8	0.0	66.4	10.2	4.7	0.1

Month	Specific energy flows - PC1b_50 - Proposed case (kWh/m^2)					
	Heating load	Cooling load	Infiltration load	Transmission load	Internal load	Solar load
Jan	71.2	0.0	63.2	13.2	5.1	0.1
Feb	55.9	0.0	49.3	11.5	4.4	0.5
Mar	38.8	0.0	34.5	10.0	4.9	0.8
Apr	31.7	0.1	28.7	9.1	4.7	1.6
May	21.5	0.6	20.7	7.3	5.1	2.0
Jun	5.6	3.1	6.5	3.0	4.7	2.4
Jul	10.3	1.1	12.0	3.9	4.9	1.9
Aug	9.3	1.6	11.2	3.2	5.1	1.6
Sep	16.5	0.5	17.2	4.2	4.5	1.0
Oct	28.9	0.2	28.3	6.1	5.1	0.6
Nov	35.4	0.0	33.5	7.0	4.8	0.2
Dec	46.3	0.0	42.0	9.1	4.7	0.0

Figure 5. Monthly specific energy flows for the building associated with RC1b and PC1b_50 case studies.

Comparing the simulation results returned for PC1b_50 with those associated with RC1b, this figure highlights that:

- the case PC1b_50 allow to reduce the monthly specific energy flows associated with the heating load; in particular, the reduction during the whole year is about 41% (257.2 kWh/m^2);
- the case PC1b_50 increases the yearly specific energy flows associated with the cooling load by about 22% (1.3 kWh/m^2); only in June (the hottest month, Figure 1) the SS system allows to reduce the monthly specific energy flows associated with the cooling load of about 35% (1.7 kWh/m^2);

Table 6: Thermal and cooling energy flows in MWh, upon varying the case study and the month.

Case study	En. flow (MWh)	Jan	Feb	Mar	Apr	May	Jun	Jul	Aug	Sep	Oct	Nov	Dec	Year
RC1a	Cooling						16.0	0.5	2.2	0.2				19.0
	Thermal	508.5	421.6	322.2	291.0	204.5	48.4	94.8	77.9	138.9	227.2	259.0	332.1	2925.9
PC1a_50	Cooling			0.1	0.5	2.5	12.7	4.9	7.1	2.5	1.0			31.3
	Thermal	336.8	264.1	185.6	153.6	104.6	26.9	50.1	44.9	79.8	137.7	167.9	219.9	1771.8
PC1a_100	Cooling				0.1	2.2	13.0	4.2	5.6	1.2	0.2			26.5
	Thermal	337.9	271.7	201.6	168.3	113.7	29.0	54.2	47.7	84.9	143.8	168.8	220.2	1842.0
PC1a_150	Cooling					1.2	13.1	2.7	3.7	0.3	0.2			21.2
	Thermal	338.4	273.1	206.7	178.7	120.7	30.0	56.8	48.6	86.6	144.8	169.1	220.4	1873.7
PC1a_200	Cooling					0.6	12.6	1.5	3.0	0.3	0.2			18.2
	Thermal	338.9	274.0	208.2	183.7	124.7	30.4	57.9	48.8	86.9	145.3	169.3	220.5	1888.5
PC1a_250	Cooling					0.6	12.7	1.2	2.9	0.3	0.2			17.9
	Thermal	339.3	274.8	209.2	185.2	126.5	30.5	58.3	48.9	87.1	145.5	169.4	220.5	1895.2
PC1a_300	Cooling					0.6	12.8	1.2	2.9	0.3	0.2			17.9
	Thermal	339.5	275.4	209.7	186.2	127.4	30.5	58.4	48.9	87.2	145.8	169.5	220.6	1899.2
RC1b	Cooling					0.2	22.2	0.9	4.0	0.2				27.5
	Thermal	509.8	423.3	320.9	284.2	197.9	47.6	91.6	76.5	137.5	227.5	259.4	332.4	2908.6
PC1b_50	Cooling			0.1	0.5	2.7	14.4	5.2	7.3	2.4	1.0			33.7
	Thermal	329.6	258.6	179.6	146.5	99.3	26.0	47.6	42.9	76.4	133.9	163.9	214.4	1718.7
PC1b_100	Cooling					2.3	14.6	4.4	5.7	1.1	0.2			28.3
	Thermal	330.6	267.9	195.5	159.5	107.5	27.9	51.4	45.3	81.2	140.7	164.6	214.6	1786.7
PC1b_150	Cooling					1.2	14.4	2.8	3.7	0.3	0.2			22.6
	Thermal	331.2	270.5	200.7	169.4	113.3	28.6	53.5	46.1	82.9	141.7	164.8	214.7	1817.5
PC1b_200	Cooling					0.6	13.7	1.5	3.1	0.3	0.2			19.3
	Thermal	331.8	271.3	202.3	174.2	117.1	29.0	54.4	46.4	83.3	142.0	164.9	214.7	1831.5
PC1b_250	Cooling					0.6	13.7	1.2	3.0	0.3	0.1			18.9
	Thermal	332.0	271.9	203.8	175.8	119.0	29.2	54.8	46.5	83.5	142.2	164.9	214.8	1838.2
PC1b_300	Cooling					0.5	13.9	1.2	2.9	0.2	0.1			18.9
	Thermal	332.2	272.5	204.6	176.9	119.9	29.2	54.9	46.5	83.6	142.3	164.9	214.8	1842.0
RC2a	Cooling					0.1	16.4	0.6	2.4	0.2				19.6
	Thermal	493.5	408.6	310.9	281.1	197.3	46.4	91.6	75.5	134.7	220.5	251.0	321.6	2832.6
PC2a_50	Cooling			0.1	0.6	3.0	13.1	5.4	7.4	2.7	1.1			33.4
	Thermal	329.0	257.1	179.6	148.6	101.4	26.1	49.1	44.2	78.7	135.1	164.3	214.6	1727.9
PC2a_100	Cooling				0.1	2.6	13.3	4.6	5.8	1.3	0.3			28.0
	Thermal	330.1	264.7	195.4	163.3	110.5	28.1	53.2	47.0	83.7	141.2	165.2	215.0	1797.3
PC2a_150	Cooling					1.4	13.4	3.0	3.8	0.3	0.2			22.1
	Thermal	330.5	266.0	200.4	173.4	117.2	29.1	55.7	47.9	85.3	142.2	165.5	215.1	1828.4
PC2a_200	Cooling					0.7	12.9	1.7	3.1	0.3	0.2			18.9
	Thermal	331.0	267.0	201.9	178.3	121.1	29.5	56.8	48.2	85.7	142.7	165.6	215.2	1843.0
PC2a_250	Cooling					0.7	12.9	1.3	3.0	0.3	0.2			18.4
	Thermal	331.5	267.8	202.9	179.8	122.8	29.6	57.2	48.3	85.9	142.9	165.8	215.2	1849.6
PC2a_300	Cooling					0.7	13.0	1.3	2.9	0.3	0.2			18.4
	Thermal	331.6	268.4	203.4	180.9	123.8	29.7	57.3	48.3	86.0	143.1	165.8	215.3	1853.7
RC2b	Cooling					0.3	22.8	1.0	4.2	0.2				28.6
	Thermal	494.8	410.3	309.6	274.3	190.7	45.7	88.4	74.1	133.3	220.8	251.4	321.9	2815.1
PC2b_50	Cooling			0.1	0.6	3.2	14.8	5.7	7.6	2.7	1.1			35.9
	Thermal	321.7	251.6	173.7	141.6	96.1	25.1	46.6	42.3	75.3	131.4	160.2	209.1	1674.8
PC2b_100	Cooling				0.1	2.7	14.9	4.8	6.0	1.2	0.2			29.9
	Thermal	322.7	260.9	189.3	154.4	104.3	27.0	50.4	44.7	80.0	138.0	161.0	209.3	1742.0
PC2b_150	Cooling					1.4	14.7	3.1	3.8	0.3	0.2			23.5
	Thermal	323.4	263.5	194.5	164.1	109.9	27.8	52.5	45.5	81.6	139.0	161.1	209.4	1772.3
PC2b_200	Cooling					0.7	14.0	1.6	3.2	0.3	0.2			19.9
	Thermal	323.9	264.2	196.1	168.8	113.5	28.2	53.4	45.8	82.0	139.4	161.2	209.5	1786.0
PC2b_250	Cooling					0.7	14.0	1.3	3.1	0.3	0.2			19.5
	Thermal	324.1	264.9	197.5	170.4	115.4	28.3	53.7	45.8	82.2	139.6	161.3	209.5	1792.7
PC2b_300	Cooling					0.6	14.1	1.3	3.0	0.3	0.1			19.5
	Thermal	324.3	265.4	198.3	171.5	116.3	28.3	53.8	45.9	82.3	139.6	161.3	209.5	1796.5

- both infiltration and transmission loads are outgoing energy flows during the whole year because, for all the months, T_{AVG} is lower than the setpoint of the indoor air temperature; using the SS system allows to reduce the infiltration load by about 44% (275 kWh/m^2), while the transmission load is reduced of about 9.9% (9.6 kWh/m^2);
- adopting the proposed SS system and control logic on the windows too allows for a reduction of about 67.5% (26.5 kWh/m^2).

Discussion and Conclusions

As reported in the literature review, there is a limited number of research activities about SS facade systems, or ventilated facades in general, in the Nordic and cold climates regions, while contemporary architecture is growingly adopting these systems, even without a proper evaluation of their effects other than the design ones. The gap widens when SS systems integrating tensile materials as outer layers are considered. In this regard, this study stands as a best-practice and control strategy suggestion for new or already existing tensile SS systems. The simulation results show that, with proper control logic, these systems are able to achieve significant results even at latitudes where the SS systems are traditionally unsuitable while also providing for design freedom and quick retrofit times. These results, along with the ones from the numerical analysis of the SS system performance, where instead an average value of PES of about 30% was achieved for all the retrofit cases, highlight a precise scenario. Considering the characteristics of the reference buildings, they may indeed be not up to standard in terms of thermal transmittances of the external surfaces; however, the reference values are not so low to motivate a retrofit action based solely on the implementation of the thermal characteristics of the envelope. Instead, the characteristics of the reference buildings highlight a need for intervention on the transparent surfaces, particularly on the infiltration rates between outdoor and indoor. For this reason, a SS system integrating a tensile material, which may effectively be installed on the whole façade (both opaque and transparent surfaces) is an easy and light way to address this weakness without the need for a complete window retrofit. In this study, the changes in infiltration rates were assumed on the basis of literature references as reported before. Moreover, at this step of the research, considering that there are no experimental data available for the SS system integrating the tensile material in Nordic regions, the numerical model for the proposed SS system was developed and validated in the south European area. In this regard, this research represents only the first step of a possible broader experimental study. In addition, the following aspects should be investigated with in-situ tests: wind resistance, decrease of daylight, influence on natural ventilation possibilities, impact of the control strategy parameters/setpoints, rain, moisture, and frost management in such a system. Therefore, the need for an experimental assessment and model validation of the thermal performances of the system in cold climates is necessary, as well as the study of the fluid dynamic behavior of the air from the cavity to the indoor environment.

References

Boermans, T., Bettgenhäuser, K., Offermann, M., & Schimschar, S. (2012). *RENOVATION TRACKS FOR EUROPE UP TO 2050 - Building renovation in Europe - what are the choices?* https://www.eurima.org/uploads/ModuleXtender/Publications/90/Renovation_tracks_for_Europe_08_06_2012_FINAL.pdf

Chen, X., Qu, K., Calautit, J., Ekambaram, A., Lu, W., Fox, C., Gan, G., & Riffat, S. (2020). Multi-criteria assessment approach for a residential building retrofit in Norway. *Energy and Buildings*, *215*. https://doi.org/10.1016/j.enbuild.2019.109668

Chiu, S. K., & Lin, E. S. (2015). Tensile Membrane Façade: Performance Analysis of Energy, Daylighting and Material Optical Properties. In Advanced Building Skins (Ed.), *10th Conference on Advanced Building Skins*. https://www.researchgate.net/publication/282650967

Cho, G.-Y., & Kim, M.-S. Y. & K.-W. (2013). Design Parameters of Double-Skin FaÇade for Improving the Performance of Natural Ventilation in High-Rise Residential Buildings. *Journal of Asian Architecture and Building Engineering*, *12*(1), 125–132. https://doi.org/10.3130/jaabe.12.125

Ciampi, G., Spanodimitriou, Y., Scorpio, M., Rosato, A., & Sibilio, S. (2021a). Energy performances assessment of extruded and 3d printed polymers integrated into building envelopes for a south Italian case study. *Buildings*, *11*(4). https://doi.org/10.3390/buildings11040141

Ciampi, G., Spanodimitriou, Y., Scorpio, M., Rosato, A., & Sibilio, S. (2021b). Energy performance of PVC-Coated polyester fabric as novel material for the building envelope: Model validation and a refurbishment case study. *Journal of Building Engineering*, *41*. https://doi.org/10.1016/j.jobe.2021.102437

CORDIS - European Commission. *Textile Architecture - Textile structures and buildings of the future - CONTEX-T project*. Retrieved April 12, 2022, from https://cordis.europa.eu/project/id/26574

Darvish, A., Eghbali, S. R., Eghbali, G., & Mahlabani, Y. G. (2020). The effects of building glass facade geometry on wind infiltration and heating and cooling energy consumption. *International Journal of Technology*, *11*(2), 235–247. https://doi.org/10.14716/ijtech.v11i2.3201

de Gracia, A., Navarro, L., Castell, A., & Cabeza, L. F. (2015). Energy performance of a ventilated double skin facade with PCM under different climates.

Energy and Buildings, *91*, 37–42. https://doi.org/10.1016/j.enbuild.2015.01.011

Diallo, T. M. O., Zhao, X., Dugue, A., Bonnamy, P., Javier Miguel, F., Martinez, A., Theodosiou, T., Liu, J. S., & Brown, N. (2017). Numerical investigation of the energy performance of an Opaque Ventilated Façade system employing a smart modular heat recovery unit and a latent heat thermal energy system. *Applied Energy*, *205*, 130–152. https://doi.org/10.1016/j.apenergy.2017.07.042

Dickson, A. (2004). *Modelling Double-Skin Facades*.

Direktoratet for byggkvalitet. *Building Acts and Regulations*. Retrieved April 12, 2022, from https://dibk.no/regelverk/Building-Regulations-in-English/

EN12831. (2003). *Heating Systems in Buildings – Method for Calculation of the Design Heat Load.*

Enova. (2004). *Manual for Enøk Normtall*. https://www.enova.no/

European Commission. (2018). *Energy performance of buildings directive*. https://energy.ec.europa.eu/topics/energy-efficiency/energy-efficient-buildings/energy-performance-buildings-directive_en

European Commission. (2021). *Climate strategies & targets*. https://ec.europa.eu/clima/policies/strategies_en

European Environment Agency. (2021). *Efficiency of conventional thermal electricity and heat production in Europe*. https://www.eea.europa.eu/data-and-maps/indicators/efficiency-of-conventional-thermal-electricity-generation-4/assessment-2

Facid North America. *Fabric Mesh Facade*. Retrieved April 12, 2022, from https://www.facidnorthamerica.com/

Gelesz, A., Catto Lucchino, E., Goia, F., Serra, V., & Reith, A. (2020). Characteristics that matter in a climate façade: A sensitivity analysis with building energy simulation tools. *Energy and Buildings*, *229*. https://doi.org/10.1016/j.enbuild.2020.110467

G.I. Industrial Holding. (2022). *TECHNICAL BROCHURE - CRA/K 15÷131*. http://www.clint.it/

Goia, F. (2016). Search for the optimal window-to-wall ratio in office buildings in different European climates and the implications on total energy saving potential. *Solar Energy*, *132*, 467–492. https://doi.org/10.1016/j.solener.2016.03.031

Gruner, M., & Haase, M. (2012). Façade-Integrated Ventilation Systems In Nordic Climate. *33rd AIVC Conference "Optimising Ventilative Cooling and Airtightness for [Nearly] Zero-Energy Buildings, IAQ and Comfort."*

Köhl, M. (2007). *Performance, durability and sustainability of advanced windows and solar components for building envelopes*.

Lehrer, D. (2011). *High-performance facades design strategies and applications in North America and Northern Europe*. https://www.researchgate.net/publication/ 336349963

Naboni, E., & Tarantino, S. (2014). The Climate Based Design of Opaque Ventilated Façades. *Conference Proceedings of the 9th ENERGY FORUM*, 1023–1030.

Nord, N., Ding, Y., Skrautvol, O., & Eliassen, S. F. (2021). Energy Pathways for Future Norwegian Residential Building Areas. *Energies*, *14*(4), 934. https://doi.org/10.3390/en14040934

Poirazis, H. (2004). *Double Skin Façades for Office Buildings Division of Energy and Building Design*.

Roselli, C., Marrasso, E., Tariello, F., & Sasso, M. (2020). How different power grid efficiency scenarios affect the energy and environmental feasibility of a polygeneration system. *Energy*, *201*. https://doi.org/10.1016/j.energy.2020.117576

Saad, M. M., & Araji, M. T. (2020). Optimization Of Double Skin Façades With Integrated Renewable Energy Source In Cold Climates. *Building Performance Analysis Conference and SimBuild*.

Schimschar, S., Grözinger, J., Korte, H., Boermans, T., Lilova, V., & Bhar, R. (2011). *Panorama of the European non-residential construction sector*. http://leonardo-energy.pl/wp-content/uploads/2018/03/Europejski-sektor-budownictwa-niemieszkalnego.pdf

Serge Ferrari (a). *Frontside View 381*. Retrieved May 12, 2020, from https://www.sergeferrari.com/products/frontside-range/frontside-view-381

Serge Ferrari (b). *Textile and bioclimatic façade*. Retrieved April 12, 2022, from https://www.sergeferrari.com/applications/bioclimatic-facade-building-construction-and-renovation

Shahrzad, S., & Umberto, B. (2022). Parametric optimization of multifunctional integrated climate-responsive opaque and ventilated façades using CFD simulations. *Applied Thermal Engineering*, *204*. https://doi.org/10.1016/j.applthermaleng.2021.117923

Soudian, S., & Berardi, U. (2021). Development of a performance-based design framework for multifunctional climate-responsive façades. *Energy and Buildings*, *231*. https://doi.org/10.1016/j.enbuild.2020.110589

UNI/TS 11300-1. (2014). *Energy Performance of Buildings Part 1: Evaluation of Energy Need for Space Heating and Cooling.*